

Automated Spectral Smoothing with Spatially Adaptive Penalized Least-Squares

Aaron A. Urbas and Steven J. Choquette

ABSTRACT

A variety of data smoothing techniques exist to address the issue of noise in spectroscopic data. The vast majority, however, require parameter specification by a knowledgeable user, which is typically accomplished by trial and error. In most situations, however, optimal parameters represent a compromise between noise reduction and signal preservation. In this work, we demonstrate a non-parametric regression approach to spectral smoothing using a spatially adaptive penalized least squares (SAPLS) approach. An iterative optimization procedure is employed that permits gradual flexibility in the smooth fit when statistically significant trends based on multiscale statistics assuming white Gaussian noise are detected. With an estimate of the noise level in the spectrum the procedure is fully automatic with a specified confidence level for the statistics. The potential application to the heteroscedastic noise case is also demonstrated. Performance was assessed in simulations using several synthetic spectra by traditional error measures as well as the modality of the resulting fits. For the simulated spectra, a best case comparison with the Savitzky-Golay smoothing method via an exhaustive parameter search was performed while the SAPLS method was assessed for automated application. The application to several dissimilar experimentally obtained Raman spectra is also presented.

INTRODUCTION

A diversity of techniques exists to address the issue of discriminating signal from noise in spectroscopic data. The now classic Savitzky-Golay (SG) method^{1,2} is one of the most popular approaches to smoothing and derivative approximation in spectroscopy and a benchmark against which novel techniques are often evaluated³⁻⁸. Most methods require parameter specification by a skilled practitioner, which is often optimized by a trial and error approach. Automation of this and other data pre-treatment techniques is desirable and many efforts towards this end have been reported in a diversity of fields. A brief literature survey relating to spectroscopy reveals automated approaches to smoothing^{7,9-12}, baseline correction¹³⁻¹⁸, spike noise detection¹⁹⁻²², and noise estimation¹⁹ among others. For smoothing applications, intrinsic properties of a given smoothing method (e.g. frequency response) impose limits on achievable noise rejection even when optimal parameters are applied, and a compromise between noise reduction and signal preservation is unavoidable.

Of principal interest in this work is the application to Raman spectroscopic data, which present challenges to smoothing as they can contain a diversity of broad and narrow spectral features compounded by baseline issues and often heteroscedastic noise. While continuous, these spectra can exhibit extreme degrees of spatially inhomogeneous smoothness. Optimal filter characteristics in this case depend on local signal dynamics and adaptive, data-driven methods can provide superior performance. There are many approaches to the general non-parametric regression problem of specifying a smooth function of unknown form to noisy data to potentially address this problem. The literature is vast and increasing, but a sampling of techniques includes traditional smoothing splines²³⁻²⁵, adaptive spline variants using local

smoothing parameters or knot/basis selection²⁶⁻³¹, local polynomials³²⁻³⁴, and wavelets³⁵⁻³⁸.

While the utility of many of these methods has been established in terms of error measures, another measure of efficacy valuable for spectral interpretation is how well true local extremes in the data are preserved while spurious extremes are minimized. Few methods explicitly address local extremes or modality and shortcomings of several popular techniques in this regard are clear^{31, 39}. The taut string functional⁴⁰⁻⁴³ is one established method to address this issue but produces a piecewise constant function in the original formulation. A smooth extension based on solving a constrained optimization problem has been proposed³⁹. In our experience, knot-selection or free-knot spline procedures also perform well in this regard but, for the spectral data under consideration at least, the computational requirements can be unreasonable (e.g. hours or even longer for a single spectrum).

In this work, we demonstrate a non-parametric regression approach to smoothing based on penalized least squares⁴⁴⁻⁴⁶ with a locally adaptive difference penalty, which we term spatially adaptive penalized least-squares (SAPLS). In brief, the method is an iterative optimization procedure balancing data fidelity and roughness until no significant trends, based on multiscale statistics assuming white Gaussian noise, are detected. We assess the capability of the method for automated implementation and demonstrate the potential application to the heteroscedastic noise case. While no explicit constraints on local extremes are incorporated, the method was found to be quite effective in this regard using one of the statistics evaluated. Performance was evaluated using several synthetic spectra with a range of noise levels and several experimentally obtained Raman spectra. As most of the readers will be familiar with

the Savitzky-Golay smoothing method, a best-case comparison in terms of error was conducted for the simulations while the SAPLS method was assessed for unsupervised application.

THEORY

Penalized Least Squares. Given an n -point data series \mathbf{y} we wish to determine a smooth series \mathbf{z} that balances two competing goals of data fidelity and roughness, which are defined here in the traditional least-squares sense and by d -order differences between adjacent data points, respectively. Explicitly, for first-order differences, a typical cost function (Q) of the two goals is expressed in Eq. 1 with a flexible penalty (λ) placed on the roughness measure.

$$Q = \sum_{i=1}^n (y_i - z_i)^2 + \lambda \sum_{j=2}^n (z_j - z_{j-1})^2 \quad \text{Eq. 1}$$

The magnitude of the roughness penalty λ regulates the trade-off between smoothness and fit to the data. The objective of penalized least squares is to determine \mathbf{z} that minimizes Q . Differences of any order may be used; however, increasing order places a limit on the smooth approximation. The limiting solution to \mathbf{z} as λ gets very large approaches a polynomial of order $d - 1$. Penalized least squares smoothing with this approach has been around for some time¹ and is more commonly known as Whittaker/Whittaker-Henderson smoothing or the Hodrick-Prescott filter depending on the order of differences used.

Following Eilers⁴⁵, minimization of the cost function Q is straightforward if matrix notation is introduced, with Eq. 1 restated as Eq. 2. The vector of partial derivatives is given in Eq. 3, and minimization of this equation is the least squares solution to the linear system of equations in Eq. 4.

$$Q = |\mathbf{y} - \mathbf{z}|^2 + \lambda |\mathbf{D}\mathbf{z}|^2 \quad \text{Eq. 2}$$

$$\frac{\partial Q}{\partial \mathbf{z}} = -2(\mathbf{y} - \mathbf{z}) + 2\lambda \mathbf{D}^T \mathbf{D}\mathbf{z} \quad \text{Eq. 3}$$

$$\mathbf{y} = (\mathbf{I} + \lambda \mathbf{D}^T \mathbf{D})\mathbf{z} \quad \text{Eq. 4}$$

where \mathbf{D} is the d -order differencing matrix, $|\cdot|^2$ indicates the vector sum of squares, \mathbf{I} is the identity matrix, and T represents the matrix transpose. This smoothing method has a number of useful attributes including no boundary constraints, ability to handle missing values and adaptability to non-uniform data point spacing. Taking advantage of the sparsity of the system, the computations are very efficient even for large data sets and efficient cross-validation methods can be used to optimize λ . A shortcoming that this technique shares with the SG method, unfortunately, is that the optimal λ in most cases represents a compromise between noise-reduction and fidelity. This work represents a method to overcome this limitation by the introduction of a locally varying difference penalty, λ_j (for $j = 1$ to $n - d$). Introduced into the cost function as a diagonal matrix $\mathbf{\Lambda}$ this yields Eq. 5 and the linear system of equations to solve becomes Eq. 6.

$$Q = |\mathbf{y} - \mathbf{z}|^2 + |\mathbf{\Lambda}\mathbf{D}\mathbf{z}|^2 \quad \text{Eq. 5}$$

$$\mathbf{y} = (\mathbf{I} + \mathbf{D}^T \mathbf{\Lambda}\mathbf{\Lambda}^T \mathbf{D})\mathbf{z} \quad \text{Eq. 6}$$

Determining “optimal” diagonal elements (λ_j) of $\mathbf{\Lambda}$ depends on the nature of the underlying model in question. The approach chosen here, which is presented in the next section, is cast in the framework of non-parametric regression based on confidence regions or sets assuming white Gaussian noise. In addition, a simple extension to the case of Poisson noise is also discussed.

An alternative approach to adaptive smoothing via penalized least squares is to introduce a variable weight parameter directly on the data points themselves (i.e. the first term in Eq. 1) while fixing the difference penalty. Spatially adaptive weighting in this manner was also investigated; however, in nearly all cases examined here the results using adaptive difference penalties were comparable or significantly better than adaptive weighting.

It serves to note here the similarity between Eq. 1 and the typical function minimized in the case of smoothing splines. A difference penalty of order d can be conceptually compared with penalizing the d -order derivative of \mathbf{z} . Smoothing splines are continuous piecewise polynomial curves with a flexible constraint (smoothing parameter) placed on the derivative. Cubic smoothing splines, for example, are piecewise cubic polynomials with constraint placed on the integrated square of the second derivative. In contrast, polynomial basis sets are not utilized in penalized least squares. However, a comparison of the fit obtained by minimizing Eq. 1 with a global second-order difference penalty yields a very similar solution to a cubic smoothing spline given that the smoothing parameters are suitably chosen.

Multiscale Statistics. The optimization procedure chosen here is an iterative algorithm based on the analysis of residuals and, as such, requires a stochastic model for statistical analysis, which we assume as Eq. 7.

$$y_i = z_i + \sigma \varepsilon_i \quad \{i = 1 \text{ to } n\} \quad \text{Eq. 7}$$

where ε is taken to be standard Gaussian white noise with mean zero and standard deviation σ .

In this work, two multiscale statistics aimed at detecting and localizing departures from Gaussian white noise in the residuals were evaluated. While thorough treatments of these statistics are beyond the current scope, concise presentations are useful to illustrate the

multiscale methodology and demonstrate how the statistics were used in the optimization procedure.

The first statistic is a nonparametric confidence region for \mathbf{z} based on normalized sums of residuals over intervals^{31, 43, 47}, which, for a specific interval, is defined in Eq. 8:

$$\omega(\mathbf{y}_n, I, g) = \frac{1}{\sqrt{|I|}} \sum_{i \in I} (y_i - g_i) \quad \text{Eq. 8}$$

where g is any function, I denotes an interval, and $|I|$ denotes the number of points in the interval I . With σ known (or estimated), a confidence region for \mathbf{z} (A_n) is defined in Eq. 9:

$$A_n = \left\{ g : \max_{I \in I_n} |\omega(\mathbf{y}_n, I, g)| \leq \sigma \sqrt{\tau_n \log n} \right\} \quad \text{Eq. 9}$$

where I_n denotes a family of intervals, and τ_n is specified based on a desired confidence level (e.g. $\alpha = 0.05$ for 95%) of the region.

Evaluation of this metric over all possible intervals, an $O(n^2)$ operation, is computationally expensive for even moderately sized data sets and Davies et al.⁴⁷ propose a parameterized multiresolution scheme that provides interval families of $O(n)$ that arbitrarily approach the case of all intervals. A dyadic interval family analogous to that for the Haar wavelet consisting of all one point intervals ($I = 1, 2, 3, \dots$), two point intervals ($I = [1, 2], [3, 4], \dots$), four point intervals ($I = [1, 2, 3, 4], [5, 6, 7, 8], \dots$), and so forth is suggested. In our experience, this interval family is adequate if the signal of interest is sufficiently sampled but denser schemes are typically necessary for sparsely sampled signals (e.g. Raman spectra). Critical τ_n values are determined by simulations and depend on both the interval scheme and number of data points. However, exact values for τ_n are not imperative in practice and the authors recommend values from 2.5 to 3.0, which approximately correspond to confidence levels in the 95% to 99% range.

In this work, simulations were carried out using a range of τ_n values from 2.0 to 2.75. To avoid concern about selection of a sufficiently dense interval family, the family of all possible intervals was used for the results presented here. Note that similar results to those reported for the simulated data were obtained with much coarser interval schemes. For conciseness we designate this statistic in the remainder of this article as MSCR (MultiScale Confidence Region).

The second metric evaluated is a multiscale trend detection test statistic based on the supremum norm of standardized kernel estimators over different locations and bandwidths⁴⁸. We forego a mathematical treatment of this statistic as it is comparatively more complex and refer interested readers to the literature. The proposed statistic tests a non-parametric qualitative hypothesis, such as monotonicity or concavity, against a general smooth alternative and identifies intervals where the null hypothesis is rejected at a specified confidence level. Several tests for qualitative hypotheses are derived in the cited work⁴⁸ and their utility was evaluated as it pertained to this application. We found the proposed test with a null hypothesis of monotonicity provided the best performance in the current context; however, this was partly based on subjective valuations of the resulting curves. The test signal, representing the kernel function in this hypothesis, is presented in the top panel of Figure 1. The one-sided test based on this function is designed to test the qualitative hypothesis of a strictly decreasing function, while the two-sided version, which we employ here, tests for a constant function. It is important to note that this qualitative hypothesis does not imply a test of " $f(x) = 0$ ". Instead, the statistic determines minimal intervals over which the null hypothesis can be rejected, i.e., where significantly increasing or decreasing trends are observed in the data at the specified confidence level.

As with the first statistic, estimated critical values ($\kappa_{n,\alpha}$) corresponding to $(1-\alpha)$ quantiles depend on the number of data points and are determined by Monte Carlo simulation. Exact values are not essential in practice and reasonable estimates can be used. Simulations covering $n = 100$ to 2000 gave 0.50-, 0.90-, and 0.95-quantile ranges of 1.15 to 1.29, 1.95 to 2.01 and 2.21 to 2.24, respectively. In the synthetic spectrum simulations values from 1 to 2 were investigated. For residual evaluation purposes, intervals with significant trends were accumulated over bandwidth and location. A graphical example of the accumulated trends ($\kappa = 2$) for a synthetic data example is presented in the bottom panel of Figure 1. The synthetic “spectrum” is composed of step functions ($X = 50$ and 100), linearly increasing/decreasing segments (left endpoints at $X = 100, 200$ and 325 with widths of 10, 25 and 50 points, respectively) and a Gaussian peak (centered at 450, $\sigma = 10$) with additive white Gaussian noise ($\sigma = 1$). Regions highlighted in grey correspond to points falling within intervals identified with significantly increasing or decreasing trends. No trends are detected within the flat portions of the data set at ± 10 , which are clearly anomalous considering the white Gaussian noise model. While not representative of a residual, per se, the example clearly demonstrates the utility of the statistic and highlights a principal distinction compared to the MSCR statistic, where all intervals deviating significantly from the Gaussian noise model are identified (i.e. testing the “ $f(x) = 0$ ” hypothesis). For conciseness, we will designate this statistic in the remainder of this article as MSQH (MultiScale Qualitative Hypothesis).

Optimization Algorithm. The proposed optimization procedure is an iterative approach motivated by Davies et al.^{31,41}. Essentially, the residuals of the current fit are evaluated with the chosen statistic and all data points are identified that lie within intervals failing the test

statistic (i.e. where the null hypothesis is rejected). The fit is updated by adjusting the difference penalties (or weights) corresponding to these sites and the process is repeated. While adaptive weight adjustments on the least squares term in Eq. 1 were investigated, in nearly every case examined here the results using adaptive difference penalties were comparable or significantly better. For the remainder of this work, therefore, we will restrict results and discussion to the adaptive difference penalty method. The optimization routine consists of the following steps:

- 1) Initialize all diagonal elements of $\mathbf{\Lambda}$ to a large value (maximal smoothing) and compute \mathbf{z} .
- 2) Evaluate the multiscale statistic (with a specified critical value) and determine data points which lie in intervals failing the test statistic.
- 3) Relax difference penalties associated with data points found in (2) by scaling (i.e. $\lambda_{j,\text{new}} = q * \lambda_j ; 0 < q < 1$).
- 4) Compute \mathbf{g} with updated $\mathbf{\Lambda}$ and go to (2) until no intervals fail test statistic.

Several notes regarding these steps are in order. The initial value of the diagonal elements of $\mathbf{\Lambda}$ is not critical given that it is sufficiently large but different starting values can give rise to slight disparities in the final fit. We use the default value of 10^8 . Updating the fit in step 3 requires a mapping of the data points (y_i) to difference penalties (λ_j). We accomplish this in a straightforward manner by updating all λ_j that include y_i as a term, which results in $d+1$ difference penalties associated with each data point (less for points at the edge). The scaling factor in step 3 is also flexible but too large a value will needlessly increase computation time, while too small a value can lead to over-fitting. We use $q = 0.5$ as the default value.

METHODS

Simulated Spectra. Simulations were carried out using three synthetic test spectra with pseudo-random noise added. For 2 of the test spectra, simulations were conducted with scaled Gaussian white noise added at 4 different levels with 20 replications at each level. Artificial noise was added based on the Poisson model for the 3rd test spectrum, which was replicated 50 times. The 3 test spectra are presented in Figure 2 overlaid on noise perturbed examples at the highest noise level considered. Test spectrum 1 is a summation of 12 Gaussian bands of varying location and width that were scaled such that each band maximum is approximately 1. Simulations were run with additive white Gaussian noise at $\sigma = 1/8$ (pictured), $1/16$, $1/32$, and $1/64$. Note that for fully resolved bands in the spectrum this corresponds to signal-to-noise ratios (SNR) of 8, 16, 32, and 64. Test spectrum 2 consisted of 26 Lorentzian bands with widths (FWHM) ranging from approximately 5 to 11 points covering a wide range of scales. This example was intended to be more representative of a real spectrum and was, in fact, generated by fitting Lorentzians to a Raman spectrum of sodium citrate in the 500 cm^{-1} to 1700 cm^{-1} Raman shift range. The spectrum was scaled to unit maximum and simulations were run with additive white Gaussian noise at $\sigma = 1/32$ (pictured), $1/64$, $1/128$, and $1/256$. Direct correspondence to SNR is not straightforward due to the broad range of band intensities. However, for the example shown in Figure 2 with $\sigma = 1/32$, the SNR ranges from 32 to 1.3, corresponding to the most and least intense bands (centered at $x = \sim 0.31$ and ~ 0.65 , respectively). Test spectrum 3 was composed of a repeating series of uniform width Gaussian bands (FWHM of approximately 7 data points) at 4 scales (peak amplitudes of approximately 5320, 2660, 1330 and 665) superimposed on a broad Gaussian background (peak amplitude of

approximately 40000, minimum at right edge of approximately 1150). Simulations were run with additive noise based on the Poisson model (with mean = $y_{i,true}$) and repeated 50 times. The example in Figure 2 is shown with the background removed to facilitate noise evaluation. The inset in the upper right corner of the figure shows the actual noise-free spectrum. The inset in the upper right corner of the figure shows the actual noise-free spectrum.

Raman Spectra. Raman spectra were obtained on a Renishaw S1000 micro-Raman spectrometer (Renishaw, Gloucestershire, UK) with excitation at either 632.8 nm or 785 nm. The spectrometer consists of a Leica DMLM microscope coupled to a 250 mm focal length imaging spectrograph. The detector is a proprietary deep depletion, thermoelectrically cooled (-70° C) CCD. Holographically ruled 1800 and 1200 groove/mm gratings were used for 632.8 nm and 785 nm excitation, respectively, and a slit width of 50 μm was used for all measurements. Raman spectra were obtained from samples of naphthalene (Fluka, purum grade, $\geq 98\%$) with 785 nm excitation and cyclohexane (Sigma-Aldrich, CHROMASOLV, $\geq 99.7\%$) with 632.8 nm excitation in glass vials using a 10X microscope objective. Raman spectra of *Bacillus cereus* ATCC 10987 spores were obtained by evaporative deposition of washed and resuspended spore preparations⁴⁹ on an aluminum substrate using a 50X objective with 785 nm excitation.

Noise Estimation. As noted above the multiscale statistics require a noise estimate for evaluation. We've encountered several similar techniques in common use for estimating Gaussian noise based on various differencing schemes that, in general, give comparable results in simulations but are all upward biased. For Gaussian noise estimates we use the value defined in the following equation⁵⁰:

$$\sigma_n = \frac{1.4826}{\sqrt{2}} \text{median}\{|y_i - y_{i-1}|, i = 2, \dots, n\} \quad \text{Eq. 10}$$

It is worth noting, however, that the method proposed by Turner et al.¹⁹ using 2nd order difference spectra followed by filtering to remove spike and/or signal artifacts showed the minimum bias from a brief survey of available methods with synthetic spectra. For the simulation with Poisson noise, a simple approach was chosen where the heteroscedastic noise was approximated as Gaussian with σ_i equal to the square-root of a five point moving average filter over the data. Residuals were scaled point-by-point by the corresponding σ_i estimates to approximate a homoscedastic white Gaussian noise model with $\sigma = 1$ for statistical analysis. Note that the Gaussian approximation to the Poisson distribution is “satisfactory” for count rates $\geq \sim 40$ but not recommended below this value.

Comparison Metrics. For the synthetic noise simulations two metrics were chosen to compare the efficacy of the smoothing techniques evaluated here. Note that while differencing based noise estimators are useful for raw signals (assuming independent noise between adjacent points) they can greatly underestimate noise levels after smoothing as noise in neighboring points typically becomes significantly correlated. The root mean square error (RMSE) was used to quantify differences between the true and estimated (smoothed) signals. To facilitate comparison these values are reported as relative root mean square errors (RRMSE), where RRMSE is defined here as the ratio of the RMSE of the added noise (which is approximately the noise standard deviation in the homoscedastic case) to the RMSE of the smoothed signal. Considering the RMSE or similar error estimates alone can conceal marked differences when

comparing smoothing algorithms. A second measure of efficacy assessed was the number of local extremes (minima/maxima) in the estimated signals compared to the true value.

For comparison with SG filters in the simulations we chose not to rely on automated data-driven parameter selection criteria (e.g. GOF metrics, generalized cross-validation,...) and instead chose the optimal estimate based on the minimum RMSE from an exhaustive grid search covering polynomial orders from 0 (i.e. moving average) to 3 and window widths from the order dependent minimum to 51 points. Optimal SG filter parameters were selected independently for each set of replicate synthetic spectra at a given noise level.

Data Analysis. All algorithms were implemented in Matlab 7 (Release 2008b, The Mathworks, Inc., Natick, MA) and all computations in this work were performed using this software. The Matlab implementation of the MSQH statistic was downloaded from the author's website. The computation platform was a PC running Windows XP with an Intel Core 2 Duo 2.66 GHz PC and 3GB of ram.

RESULTS & DISCUSSION

Simulated Spectra. The compiled RRMSE and local extreme data for the 3 synthetic spectrum simulations is presented in Tables 1, 2 and 3. There are several noteworthy trends within the tabulated data. The RMSE optimal SG filters were, in all cases, 2nd order polynomials with window width varying between 5 and 13 points. As would be expected, window width was directly correlated to the noise level in the spectrum. The SAPLS signal estimates using either multiscale test statistic exhibit far fewer local extremes compared with the optimal SG filters.

However, this improvement is not accompanied by considerable RMSE improvements. In fact, the RMSE optimal SG filter outperforms the SAPLS estimates in several cases, although it depends on the particular critical value chosen for each test statistic. Furthermore, the SAPLS estimates using either test statistic exhibit greater variability for replicate runs versus the SG filters. This is not surprising given that the SG filter parameters were fixed for a given permutation of test spectrum and noise level. It serves to note that, to a point, lowering the critical values below those reported in the table gave increasingly better RMSEs for the synthetic spectra considered here. However, in addition to a marked increase in variance between replicates and an overall number of local extremes, examination of the resulting estimates showed a progressively more severe qualitative deterioration manifested primarily as sharp, highly localized anomalies.

Considering the first test spectrum (see Table 1), the performance of the SAPLS algorithm using the two multiscale test statistics is comparable in terms of RMSEs but an increasing trend in the number of local extremes is evident for the MSCR based implementation as the noise level falls. This progression becomes particularly acute with the second test spectrum (see Table 2) and adjusting the critical threshold value for this statistic (τ_n) does little to alleviate the effect. It should be noted that this drawback is not an inherent limitation of the statistic but, instead, how it is utilized in the optimization procedure. Presented in Figure 3 is an example of test spectrum 1 with additive Gaussian noise ($\sigma = 1/8$) and the resulting smoothed data using the SAPLS algorithm with each multiscale statistic and the RMSE optimal SG filter. A dramatic improvement in noise rejection is evidenced in both SAPLS estimates while signal integrity is preserved to a great extent. The sharp peaks are attenuated to some

degree in all three smoothed spectra, but slightly more in the SAPLS smoothed signals. From a qualitative evaluation, however, one might expect a significant improvement in RMSE for the SAPLS estimates, which is not observed. This result becomes clear when examining the residuals of the smoothed versus true and noise perturbed signals, which are presented in Figure 4. The residuals between the true and smoothed signals for both SAPLS implementations exhibit significantly more deviation than the SG filter result for the two groups of moderately narrow bands but similar errors for the sharpest group of bands. While the SAPLS estimates excel at noise rejection for the broad bands, the low frequency deviations from the true signal contribute significantly to the RMSE. The residuals between the smoothed and noise perturbed signals of the SAPLS smoothed signals, however, appear quite random with some slightly discernible trends. In view of the noise level (shown at $\pm 2\sigma$ in Figure 4) it is certainly not simple to establish the significance of these features.

This highlights one aspect of the iterative optimization procedure used here. The SAPLS estimate gradually develops greater local flexibility at each pass but stops when the residuals just fall within “confidence bounds” at a specified level. It is easy to recognize that this can result in residuals with numerous latent trends within the Gaussian noise model that lie at the fringe of statistical significance. In our experience this mainly impacts sparsely sampled features at low signal-to-noise level. For test spectrum 2 (Table 2) the number of local extremes at the highest noise level for the SAPLS-MSQH estimates is well below the true value for the spectrum. The tabulated data is misleading for the MSCR method in this column due to the consistent introduction of artificial local extremes near the most intense bands. At this noise level, exactly half of the peaks present in the spectrum were at SNRs between 1.3 than

2.5. Many of these peaks were consistently missed in the estimates at the $\sigma = 1/32$ level and several at the $\sigma = 1/64$ level using either metric. The MSCR method was slightly better in RMSE terms for this spectrum at all noise levels but at the expense of introducing artificial extremes in the estimate. The results on test spectrum 3 (Table 3) were comparable between the two multiscale statistics. The tabulated data for local extremes is, again, slightly misleading for the MSCR method. For either statistic, the local minima/maxima associated with the weak bands centered at $x \approx 0.44$ and $x \approx 0.66$ (refer to Figure 2) were consistently missed. However, these features were easily identifiable in simple difference estimates of the first derivative.

Raman Spectra. While the simulations above were designed to assess the performance of the SAPLS algorithm on synthetic spectra representing a range of characteristics and noise levels, real spectra better serve to demonstrate the effectiveness as well as potential limitations of the method. In simulation, the RMSE optimal SG filters were selected to provide a best case comparison. Obviously, this is not possible in practice and parameters are typically optimized by the investigator. However, procedures for automatically selecting filter parameters have been offered. A recent method proposed involves the iterative application of a Savitzky-Golay filter (also known as a Kolmogorov-Zurbenko filter) until stopping criteria based on the χ^2 statistic is reached¹¹. The authors suggest zero-order, three point (i.e. moving average) or second-order, five point filters and a threshold for the stopping criteria as the number of data points. The χ^2 statistic used is

$$\chi^2 = \sum_{i=1}^n \frac{(y_i - z_i)^2}{\sigma^2} \quad \text{Eq. 12}$$

where n is the number of points, y_i are the original data points, z_i are the smoothed/filtered points, and σ is the noise level, which must be estimated if not known, of the original data. We used this method was to generate filtered data in an unsupervised manner for comparison.

For the MSQH statistic the results in Tables 1, 2 and 3 suggest using $\kappa = 1$ or even less ($\alpha \approx 0.5$) may be advantageous as it afforded considerable RMSE improvements without introducing a significant number of spurious extremes. For real spectra, however, this is not typically the case. In our experience, a κ value of 2 is effective for approximating data while minimizing spurious extremes given that the noise is effectively approximated as Gaussian. For all the Raman spectra here this value was used. For the MSCR statistic, a value of $\tau = 2.5$ was used for real data.

Presented in Figure 5, panel A is a Raman spectrum of cyclohexane with fairly poor SNR collected with 632.8 nm excitation and consisting of 3990 points. Note that the spectrum quality was deliberately diminished by attenuating the excitation laser power for the purpose of evaluating the smoothing algorithms. This noise level, however, is not atypical for many samples. Figure 5, panel B shows the resulting smoothed signals, with the strongest peaks clipped to facilitate comparison, from the SAPLS algorithm employing each multiscale statistic as well as an automated SG filter. The 2nd order, 5 point iterative SG filter provided a better result in our estimation for this spectrum and that result is shown here. The χ^2 stopping criterion was exceeded on the eighth iteration for the SG filter. Panel C of Figure 5 show the residuals with the estimated noise level denoted as dashed-lines at $\pm 2\sigma_n$, where Equation 10 was used for approximation. As evident in the raw spectrum and residuals, the noise is not homoscedastic and differs roughly by a factor of 2 in the baseline region at opposing ends of

the spectrum. The iterative SG filter provides moderate noise reduction but significant attenuation of the 801 cm^{-1} band is clearly observed in the residuals (see Panel C). The SAPLS-MSQH estimate exhibits excellent noise rejection in the lower wavenumber half of the spectrum, but various sharp anomalies, although minor, are observed in the higher wavenumber region, particularly above 3000 cm^{-1} . In this region the noise level is nearly twice the homoscedastic estimate provided by Equation 10 and emphasizes the necessity for accurate noise estimation. The SAPLS-MSCR method exhibits inconsistent noise rejection. The noise reduction is very similar to the SG filter near the 801 cm^{-1} band but improves, to a degree, at data points distant from this. This highlights a considerable shortcoming of the optimization procedure using this statistic. The influence of the strong 801 cm^{-1} band on the two SAPLS methods can be assessed in Panel D of Figure 5, which shows the difference between the estimates of the full spectrum and an abridged version with a 50 point segment encompassing the 801 cm^{-1} band removed from the spectrum (grey region). Care was taken to ensure a continuous baseline transition between the joined segments and the noise estimate was effectively identical between the two spectra. In contrast to panel C, the estimated noise level is drawn at $\pm \sigma_n$. The impact of this band on the signal estimate in neighboring regions is substantial and extends over a very wide window with the MSCR method. In contrast, removing the 801 cm^{-1} band has significantly less impact on the MSQH estimate. Considering the noise level, the disparities are minor and, with the exception of some slight peak intensity differences, are primarily associated with the shape of the baseline. The inconsistent results from the MSCR statistic, at least as utilized in the SAPLS optimization procedure, preclude implementation in an unsupervised manner for Raman spectra. This is unfortunate because

similar results to those obtained in the simulations were found using much coarser (and consequently, much faster) interval schemes. The problems encountered, however, were largely manifest in relation to relatively sharp, intense bands and this method can perform quite effectively for other types of spectral data, which has been demonstrated previously^{31, 41}. For the remaining examples we restrict the results to those from the SAPLS algorithm using the MSQH statistic.

For unsupervised application, effectiveness on signals of higher S/N is also a necessity. Presented in Figure 6 is an example of the SAPLS (MSQH) estimate for a 785 nm Raman spectrum of naphthalene. The residuals (top panel) exhibit no unusual deviations and the expanded view of the baseline region (bottom panel) reveals excellent noise rejection while preserving weak bands. For this spectrum, an iterative second order, five point SG filter exceeds the stopping criteria after 2 iterations with obvious, though minor, distortion of the prominent bands but little noise reduction.

Finally, we present one more example in Figure 7 to illustrate the potential utility of the SAPLS method in the heteroscedastic noise case. Estimating heteroscedastic noise is not straightforward and the simple procedure used in the simulations for a Poisson model would typically not be useful in practice. While we are still evaluating robust methods for variance function estimation, here we use a smooth cubic spline fit to the piecewise estimate suggested by Turner, et. al.¹⁹ The details of this procedure are beyond the current scope and the heteroscedastic estimation procedure is not automated. Presented in the top panel of Figure 7 is a background subtracted (manually) 785 nm Raman spectrum of *Bacillus cereus* spores deposited on an aluminum substrate with the raw spectrum shown in the inset. The noise

level, which is dominated by shot noise associated with autofluorescence, varies by approximately an order of magnitude across the spectrum. Under a homoscedastic noise assumption and estimate, the SAPLS result is quite coarse in the high background region where noise is under estimated and overly smooth in the low background regions where noise is over estimated (data not shown). The bottom panel of Figure 7 shows the SAPLS (MSQH) estimate of the spectrum overlaid on the baseline corrected spectrum using the heteroscedastic estimate. The same baseline was subtracted from the raw and smoothed data. All clearly discernible features in the spectrum have been preserved while affording excellent noise rejection across the spectrum. A similar procedure alleviates the over fitting that is clearly noticeable in the high Raman shift region ($> 3000 \text{ cm}^{-1}$) for the MSQH estimate in the cyclohexane example presented in panel 2 of Figure 5. In the naphthalene example (Figure 6), the estimate is very similar under either method of noise estimation.

Limitations. As implemented, the method proposed here requires that noise is normally distributed with zero mean. With properly scaled residuals, the potential to extend this to the heteroscedastic case was also demonstrated assuming that the underlying process can be approximated by a Gaussian model (e.g. Poisson noise of sufficient counts). Deviations from these assumptions, however, such as spike noise or detector defects, have not been addressed here. There have been several methods proposed for automated spike noise detection, however, and these could be used to augment this method¹⁹⁻²². In addition, implementations using non-parametric multiscale statistics (e.g. signed ranks^{51, 52}) are feasible, where explicit knowledge of the noise distribution is not required.

A practical shortcoming to the SAPLS algorithm is computation time. The MSQH statistic is an $O(n^2)$ operation, and becomes prohibitively expensive as the number of data points increases. Computation time is a function of both the number of data points and the number of iterations required before convergence, which is largely dependent on signal dynamics. For reference, the real Raman spectra presented in Figures 5 through 7 required up to ~ 10 seconds to complete on the PC platform used in this work. One notable advantage of the MSCR statistic is the potential use of relatively coarse multiscale interval scheme, which dramatically reduces computational burden.

This algorithm is not intended or appropriate as a general preprocessing smoothing technique. Computational considerations aside, the adaptive nature of the proposed algorithm (and adaptive smoothing in general) renders it unsuitable for some post processing procedures, e.g. multivariate calibration. This is not the case for conventional implementations of other popular smoothing methods (e.g. Savitzky-Golay, wavelets,...), which are linear transforms and have been used quite successfully in this realm.

CONCLUSIONS

A non-parametric regression approach to spectral smoothing using an iteratively optimized spatially adaptive penalized least squares approach was demonstrated. Given an estimate of the noise level in the spectrum the procedure is fully automated with a specified confidence level for the statistics. Existing automated methods for estimating white Gaussian noise proved sufficient in the homoscedastic case. The potential extension of this method to heteroscedastic noise case was also demonstrated given that the underlying noise model could

be approximated as a locally varying Gaussian process. However, robust variance function estimators suitable for unsupervised application are still under evaluation. In simulation, the method offered comparable RMSE measures to best case Savitzky-Golay smoothing. The effectiveness of the method on several dissimilar real Raman spectra was also presented. The modality of the resulting SAPLS smoothed signals using a multiscale qualitative hypothesis metric were in very good agreement to the true underlying signal with the notable exception of very low SNR features. This is in stark contrast to many commonly used smoothing approaches and could be very useful in automated spectral interpretation applications.

REFERENCES

1. Savitzky, A. and M.J.E. Golay, *Smoothing and Differentiation of Data by Simplified Least Squares Procedures*. Analytical Chemistry, **1964**. 36(8): p. 1627-&.
2. Gorry, P.A., *General Least-Squares Smoothing and Differentiation by the Convolution (Savitzky-Golay) Method*. Analytical Chemistry, **1990**. 62(6): p. 570-573.
3. Komsta, L., *A comparative study on several algorithms for denoising of thin layer densitograms*. Analytica Chimica Acta, **2009**. 641(1-2): p. 52-58.
4. Clupek, M., P. Matejka, and K. Volka, *Noise reduction in Raman spectra: Finite impulse response filtration versus Savitzky-Golay smoothing*. Journal of Raman Spectroscopy, **2007**. 38(9): p. 1174-1179.
5. Barclay, V.J., R.F. Bonner, and I.P. Hamilton, *Application of wavelet transforms to experimental spectra: Smoothing, denoising, and data set compression*. Analytical Chemistry, **1997**. 69(1): p. 78-90.
6. Mittermayr, C.R., S.G. Nikolov, H. Hutter, and M. Grasserbauer, *Wavelet denoising of Gaussian peaks: A comparative study*. Chemometrics and Intelligent Laboratory Systems, **1996**. 34(2): p. 187-202.
7. Schulze, H.G., R.B. Foist, A.I. Jirasek, A. Ivanov, and R.F.B. Turner, *Two-point maximum entropy noise discrimination in spectra over a range of baseline offsets and signal-to-noise ratios*. Applied Spectroscopy, **2007**. 61(2): p. 157-164.
8. Schulze, H.G., R.B. Foist, A. Ivanov, and R.F.B. Turner, *Chi-squared-based filters for high-fidelity signal-to-noise ratio enhancement of spectra*. Applied Spectroscopy, **2008**. 62(8): p. 847-853.
9. Vivo-Truyols, G. and P.J. Schoenmakers, *Automatic selection of optimal Savitzky-Golay smoothing*. Analytical Chemistry, **2006**. 78(13): p. 4598-4608.
10. Browne, M., N. Mayer, and T.R.H. Cutmore, *A multiscale polynomial filter for adaptive smoothing*. Digital Signal Processing, **2007**. 17(1): p. 69-75.
11. Schulze, H.G., R.B. Foist, A. Ivanov, and R.E.B. Turner, *Fully Automated High-Performance Signal-to-Noise Ratio Enhancement Based on an Iterative Three-Point Zero-Order Savitzky-Golay Filter*. Applied Spectroscopy, **2008**. 62(10): p. 1160-1166.
12. van der Heide, P., X.P. Xu, B.J. Marsh, D. Hanein, and N. Volkmann. *Efficient automatic noise reduction of electron tomographic reconstructions based on iterative median filtering*. in *3rd International Conference on Structural Analysis of Supramolecular Assemblies by Hybrid Methods*. **2006**. Lake Tahoe, CA.
13. Gornushkin, I.B., P.E. Eagan, A.B. Novikov, B.W. Smith, and J.D. Winefordner, *Automatic correction of continuum background in laser-induced breakdown and Raman spectrometry*. Applied Spectroscopy, **2003**. 57(2): p. 197-207.
14. Lieber, C.A. and A. Mahadevan-Jansen, *Automated method for subtraction of fluorescence from biological Raman spectra*. Applied Spectroscopy, **2003**. 57(11): p. 1363-1367.
15. Schulze, G., A. Jirasek, M.M.L. Yu, A. Lim, R.F.B. Turner, and M.W. Blades, *Investigation of selected baseline removal techniques as candidates for automated implementation*. Applied Spectroscopy, **2005**. 59(5): p. 545-574.

16. Brandt, N.N., O.O. Brovko, A.Y. Chikishev, and O.D. Paraschuk, *Optimization of the rolling-circle filter for Raman background subtraction*. Applied Spectroscopy, **2006**. 60(3): p. 288-293.
17. Cobas, J.C., M.A. Bernstein, M. Martin-Pastor, and P.G. Tahoces, *A new general-purpose fully automatic baseline-correction procedure for 1D and 2D NMR data*. Journal of Magnetic Resonance, **2006**. 183(1): p. 145-151.
18. Cao, A., A.K. Pandya, G.K. Serhatkulu, R.E. Weber, H. Dai, J.S. Thakur, *et al.*, *A robust method for automated background subtraction of tissue fluorescence*. Journal of Raman Spectroscopy, **2007**. 38(9): p. 1199-1205.
19. Schulze, H.G., M.M.L. Yu, C.J. Addison, M.W. Blades, and R.F.B. Turner, *Automated estimation of white Gaussian noise level in a spectrum with or without spike noise using a spectral shifting technique*. Applied Spectroscopy, **2006**. 60(7): p. 820-825.
20. Katsumoto, Y. and Y. Ozaki, *Practical algorithm for reducing convex spike noises on a spectrum*. Applied Spectroscopy, **2003**. 57(3): p. 317-322.
21. Takeuchi, H., S. Hashimoto, and I. Harada, *Simple and efficient method to eliminate spike noise from spectra recorded on charge-coupled device detectors*. Applied Spectroscopy, **1993**. 47(1): p. 129-131.
22. Zhang, D.M., K.N. Jallad, and D. Ben-Amotz, *Stripping of cosmic spike spectral artifacts using a new upper-bound spectrum algorithm*. Applied Spectroscopy, **2001**. 55(11): p. 1523-1531.
23. Craven, P. and G. Wahba, *Smoothing noisy data with spline functions - Estimating the correct degree of smoothing by the method of generalized cross-validation*. Numerische Mathematik, **1979**. 31(4): p. 377-403.
24. Wahba, G., *A comparison of GCV and GML for choosing the smoothing parameter in the generalized spline smoothing problem*. Annals of Statistics, **1985**. 13(4): p. 1378-1402.
25. Green, P.J.S., B. W., *Nonparametric Regression and Generalized linear Models: A roughness penalty approach*. Monographs on Statistics and Applied Probability. Vol. 58. **1993**, London: Chapman & Hall.
26. Friedman, J.H., *Multivariate Adaptive Regression Splines*. Annals of Statistics, **1991**. 19(1): p. 1-67.
27. Eilers, P.H.C. and B.D. Marx, *Flexible smoothing with B-splines and penalties*. Statistical Science, **1996**. 11(2): p. 89-102.
28. Luo, Z. and G. Wahba, *Hybrid adaptive splines*. Journal of the American Statistical Association, **1997**. 92(437): p. 107-116.
29. Miyata, S. and X.T. Shen, *Adaptive free-knot splines*. Journal of Computational and Graphical Statistics, **2003**. 12(1): p. 197-213.
30. Pintore, A., P. Speckman, and C.C. Holmes, *Spatially adaptive smoothing splines*. Biometrika, **2006**. 93(1): p. 113-125.
31. Davies, P.L. and M. Meise, *Approximating data with weighted smoothing splines*. Journal of Nonparametric Statistics, **2008**. 20(3): p. 207-228.
32. Fan, J.Q. and I. Gijbels, *Data-driven bandwidth selection in local polynomial fitting - Variable bandwidth and spatial adaptation*. Journal of the Royal Statistical Society Series B-Methodological, **1995**. 57(2): p. 371-394.

33. Fan, J.Q., N.E. Heckman, and M.P. Wand, *Local polynomial kernel regression for generalized linear-models and quasi-likelihood functions*. Journal of the American Statistical Association, **1995**. 90(429): p. 141-150.
34. Fan, J.Q., I. Gijbels, T.C. Hu, and L.S. Huang, *A study of variable bandwidth selection for local polynomial regression*. Statistica Sinica, **1996**. 6(1): p. 113-127.
35. Donoho, D.L., *De-noising by soft-thresholding*. Ieee Transactions on Information Theory, **1995**. 41(3): p. 613-627.
36. Donoho, D.L. and I.M. Johnstone, *Adapting to unknown smoothness via wavelet shrinkage*. Journal of the American Statistical Association, **1995**. 90(432): p. 1200-1224.
37. Ogden, T. and E. Parzen, *Data dependent wavelet thresholding in nonparametric regression with change-point applications*. Computational Statistics & Data Analysis, **1996**. 22(1): p. 53-70.
38. Hall, P. and P. Patil, *On the choice of smoothing parameter, threshold and truncation in nonparametric regression by non-linear wavelet methods*. Journal of the Royal Statistical Society Series B-Methodological, **1996**. 58(2): p. 361-377.
39. Kovac, A., *Smooth functions and local extreme values*. Computational Statistics & Data Analysis, **2007**. 51(10): p. 5155-5171.
40. Kovac, A., *Robust nonparametric regression and modality*, in *Developments in Robust Statistics*, R. Dutter, et al., Editors. **2003**. p. 218-227.
41. Davies, P.L., U. Gather, M. Meise, D. Mergel, and T. Mildenerger, *Residual-based localization and quantification of peaks in x-ray diffractograms*. Annals of Applied Statistics, **2008**. 2(3): p. 861-886.
42. Dumbgen, L. and A. Kovac, *Extensions of smoothing via taut strings*. Electronic Journal of Statistics, **2009**. 3: p. 41-75.
43. Davies, P.L. and A. Kovac, *Local extremes, runs, strings and multiresolution - Rejoinder*. Annals of Statistics, **2001**. 29(1): p. 61-65.
44. Whittaker, E.T., *On the theory of graduation*. Proc. Edinburgh Math. Soc., **1924**. 44: p. 77-83.
45. Eilers, P.H.C., *A perfect smoother*. Analytical Chemistry, **2003**. 75(14): p. 3631-3636.
46. Hodrick, R.J. and E.C. Prescott, *Postwar U.S. Business Cycles: An Empirical Investigation*. Journal of Money, Credit and Banking, **1997**. 29(1): p. 1-16.
47. Davies, P.L., A. Kovac, and M. Meise, *Nonparametric Regression, Confidence Regions and Regularization*. Annals of Statistics, **2009**. 37(5B): p. 2597-2625.
48. Dumbgen, L. and V.G. Spokoiny, *Multiscale testing of qualitative hypotheses*. Annals of Statistics, **2001**. 29(1): p. 124-152.
49. Schaeffe.P, J. Millet, and J.P. Aubert, *CATABOLIC REPRESSION OF BACTERIAL SPORULATION*. Proceedings of the National Academy of Sciences of the United States of America, **1965**. 54(3): p. 704-&.
50. Davies, P.L. and A. Kovac, *Local extremes, runs, strings and multiresolution*. Annals of Statistics, **2001**. 29(1): p. 1-48.
51. Dumbgen, L., *Application of local rank tests to nonparametric regression*. Journal of Nonparametric Statistics, **2002**. 14(5): p. 511-537.
52. Rohde, A., *Adaptive goodness-of-fit tests based on signed ranks*. Annals of Statistics, **2008**. 36(3): p. 1346-1374.

LIST OF TABLES

Table 1. Comparison of results for the SAPLS methods using both test statistics at several confidence levels and the RMSE optimal SG filter for synthetic test spectrum 1 at various noise levels.

Table 2. Comparison of results for the SAPLS methods using both test statistics at several confidence levels and the RMSE optimal SG filter for synthetic test spectrum 2 at various noise levels.

Table 3. Comparison of results for the SAPLS methods using both test statistics at several confidence levels and the RMSE optimal SG filter for synthetic test spectrum 3 with additive Poisson noise.

FIGURE CAPTIONS

Figure 1. Top panel: The test signal used in the multiscale qualitative hypothesis (MSQH) statistic. Bottom panel: Synthetic data set (dashed line) with additive white Gaussian noise ($\sigma = 1$) and the accumulated intervals (grey highlighted regions) exhibiting significantly increasing/decreasing trends identified with the MSQH with $\kappa = 2$. Note that σ was explicitly specified in this example and not estimated.

Figure 2. The three synthetic test spectra used in the simulations overlaid on noise perturbed examples. For spectra 1 and 2, the examples represent noise at the highest level considered. The example for spectrum 3, with additive noise based on the Poisson distribution, is shown with the background subtracted. The true spectrum is shown in the inset in the upper right corner.

Figure 3. Example of the smoothed signals from the SAPLS method using both test statistics and the RMSE optimal SG filter (2nd order, 13 point window). Values of τ and κ used were 2.5 and 2 for the MSCR and MSQH statistics, respectively. The bottom trace shows the true signal overlaid on the noise perturbed example used.

Figure 4. Residual between the smoothed and both the true signal (top trace in each panel) and noise perturbed signal (bottom trace in each panel) for the example shown in Figure 3. Estimated noise level is designated by dashed lines in the bottom trace of each panel at $\pm 2\sigma$.

Figure 5. Panel A: Raw 632.8 nm Raman spectrum of cyclohexane comprised of 3990 points. Panel B: Comparison of smoothed signals generated with the SAPLS method using the MSCR ($\tau = 2.5$) and MSQH ($\kappa = 2$) statistics and an automated SG filter. Panel C: Residual between the smoothed signals (see Panel B) and the raw spectrum. Estimated homoscedastic noise level is designated by dashed lines at $\pm 2\sigma$. Panel D: Difference between the resulting SAPLS estimates from both statistics with and without the 801 cm^{-1} band present in the spectrum. Estimated homoscedastic noise level is designated by dashed lines at $\pm 1\sigma$.

Figure 6. SAPLS smoothed 785 nm Raman spectrum of naphthalene using the MSQH ($\kappa = 2$) statistic and a homoscedastic noise estimate. The top panel shows the full intensity scale and the bottom panel highlights the baseline.

Figure 7. Top panel: Raw (inset) and baseline corrected 785 nm Raman spectrum of *Bacillus cereus* spores. Bottom panel: SAPLS smoothed result using the MSQH ($\kappa = 2$) statistic and a heteroscedastic noise estimate. The main figure is an expanded view of the fingerprint region while the inset shows the $-\text{CH}$ region.

Table 1. Comparison of results for the SAPLS methods using both test statistics at several confidence levels and the RMSE optimal SG filter for synthetic test spectrum 1 at various noise levels.

Method	Critical Value	Figure-of-Merit	Noise Level (σ) ^a			
			1/8	1/16	1/32	1/64
MSQH	$\kappa = 1.0$	RRMSE ^b	2.49 (0.19)	2.14 (0.15)	2.02 (0.16)	1.72 (0.09)
		Extremes ^{c,d}	24 [22,26]	23 [23,27]	25 [24,28]	25 [24,28]
	$\kappa = 1.5$	RRMSE Extremes	2.25 (0.14) 23 [21,26]	1.97 (0.14) 23 [23,26]	1.80 (0.13) 25 [23,29]	1.53 (0.10) 25 [23,29]
	$\kappa = 2.0$	RRMSE Extremes	2.07 (0.15) 23 [21,25]	1.84 (0.14) 23 [23,26]	1.70 (0.12) 25 [23,27]	1.40 (0.07) 25 [23,26]
MSCR	$\tau = 2.0$	RRMSE Extremes	2.25 (0.14) 26 [21,28]	1.91 (0.13) 32 [27,39]	1.82 (0.14) 41 [34,47]	1.62 (0.11) 46 [39,56]
	$\tau = 2.5$	RRMSE Extremes	2.04 (0.12) 24 [21,27]	1.74 (0.12) 30.5 [26,36]	1.62 (0.11) 37.5 [34,43]	1.43 (0.08) 45 [40,54]
	$\tau = 2.75$	RRMSE Extremes	1.95 (0.12) 23 [21,26]	1.66 (0.10) 30 [24,33]	1.55 (0.08) 37.5 [34,42]	1.37 (0.06) 43 [39,52]
Savitzky-Golay	N/A	RRMSE	2.15 (0.09)	1.86 (0.06)	1.69 (0.06)	1.55 (0.04)
		Extremes	359.5 [310,390]	341 [309,385]	321.5 [306,348]	246 [227,267]
		Order	2	2	2	2
		Width	13	9	7	7

- a) Data compiled from 20 replications at each noise level.
- b) Table entries correspond to mean (std. dev.).
- c) Table entries correspond to median [min,max].
- d) The noise free spectrum is characterized by 23 local extremes enumerated here by sign changes in the first difference spectrum.

Table 2. Comparison of results for the SAPLS methods using both test statistics at several confidence levels and the RMSE optimal SG filter for synthetic test spectrum 2 at various noise levels.

Method	Critical Value	Figure-of-Merit	Noise Level (σ) ^a			
			1/32	1/64	1/128	1/256
MSQH	$\kappa = 1.0$	RRMSE ^b	1.93 (0.11)	1.66 (0.10)	1.48 (0.08)	1.27 (0.07)
		Extremes ^{c,d}	33 [27,41]	45 [39,52]	55.5 [49,60]	56 [51,61]
	$\kappa = 1.5$	RRMSE	1.78 (0.09)	1.52 (0.08)	1.35 (0.06)	1.17 (0.07)
		Extremes	29 [25,37]	41 [35,49]	54 [49,56]	55 [51,59]
	$\kappa = 2.0$	RRMSE	1.66 (0.08)	1.39 (0.08)	1.25 (0.05)	1.08 (0.05)
		Extremes	27 [25,33]	39 [33,45]	52 [43,54]	54 [52,59]
MSCR	$\tau = 2.0$	RRMSE	1.99 (0.10)	1.71 (0.07)	1.53 (0.07)	1.35 (0.06)
		Extremes	55 [49,69]	99 [90,118]	134 [116,159]	162.5 [144,184]
	$\tau = 2.5$	RRMSE	1.86 (0.10)	1.60 (0.07)	1.41 (0.06)	1.26 (0.06)
		Extremes	47 [42,61]	91.5 [74,108]	125 [110,147]	155 [140,166]
	$\tau = 2.75$	RRMSE	1.80 (0.09)	1.54 (0.07)	1.37 (0.06)	1.22 (0.05)
		Extremes	46 [40,57]	86 [74,105]	121 [106,139]	153 [134,166]
Savitzky-Golay	N/A	RRMSE	1.87 (0.04)	1.64 (0.03)	1.48 (0.03)	1.37 (0.03)
		Extremes	473 [443,496]	455.5 [425,501]	405 [384,458]	423 [400,447]
		Order	2	2	2	2
		Width	9	7	7	5

a) Data compiled from 20 replications at each noise level.

b) Table entries correspond to mean (std. dev.).

c) Table entries correspond to median [min,max].

d) The noise free spectrum is characterized by 51 local extremes enumerated here by sign changes in the first difference spectrum.

Table 3. Comparison of results for the SAPLS methods using both test statistics at several confidence levels and the RMSE optimal SG filter for synthetic test spectrum 3 with additive Poisson noise.

Method	Critical Value	Figure-of-Merit ^a	
MSQH	$\kappa = 1.0$	RRMSE ^b Extremes ^{c,d}	1.80 (0.12) 29 [27,31]
	$\kappa = 1.5$	RRMSE Extremes	1.65 (0.10) 29 [27,31]
	$\kappa = 2.0$	RRMSE Extremes	1.49 (0.09) 27 [27,31]
MSCR	$\tau = 2.0$	RRMSE Extremes	1.57 (0.08) 32 [27,37]
	$\tau = 2.5$	RRMSE Extremes	1.45 (0.08) 31 [27,37]
	$\tau = 2.75$	RRMSE Extremes	1.39 (0.07) 29 [27,37]
Savitzky-Golay	N/A	RRMSE Extremes Order Width	1.87 (0.07) 175 [155,202] 2 9

- a) Data compiled from 50 replications.
- b) Table entries correspond to mean (std. dev.).
- c) Table entries correspond to median [min,max].
- d) The noise free spectrum is characterized by 31 local extremes enumerated here by sign changes in the first difference spectrum.

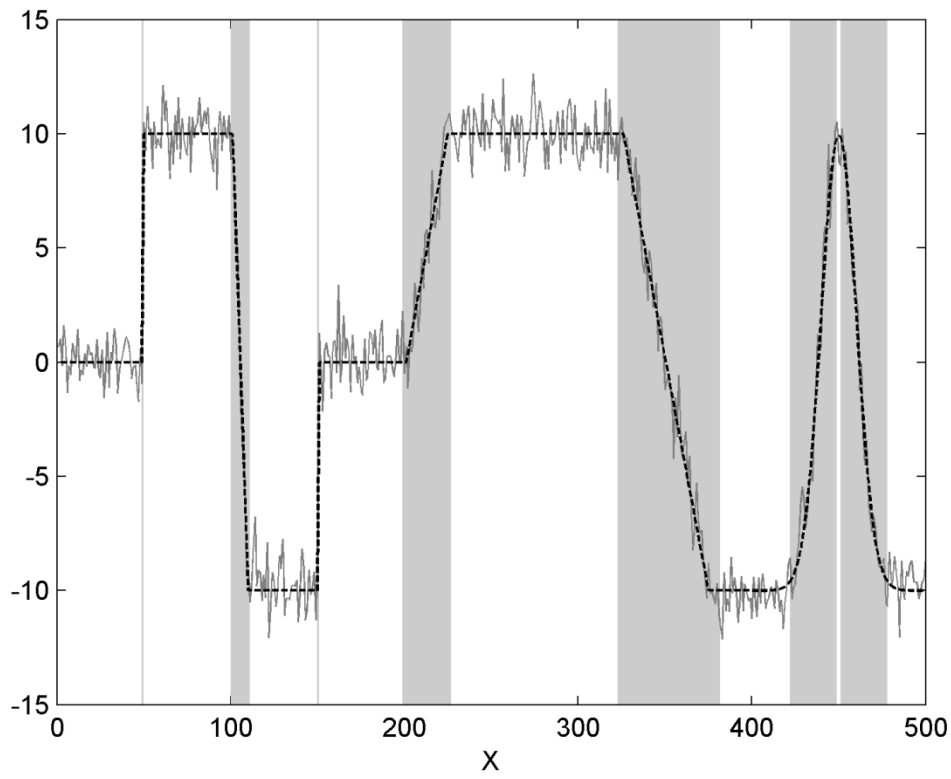
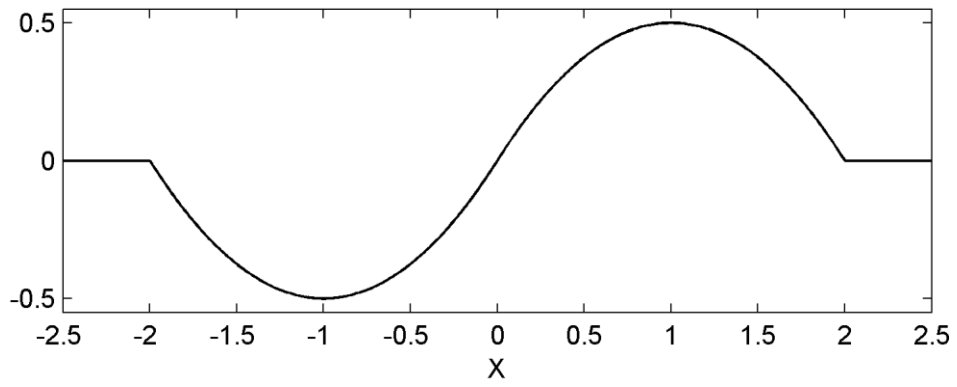


Figure 1.

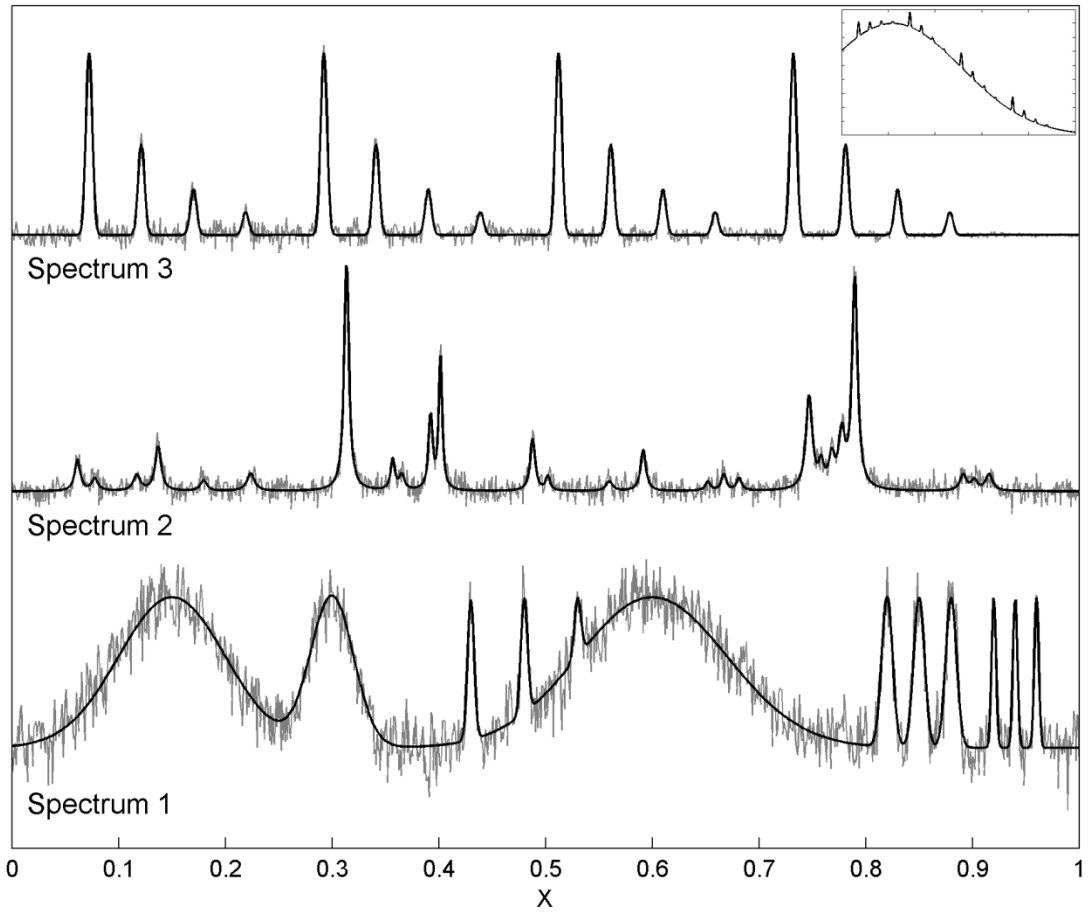


Figure 2.

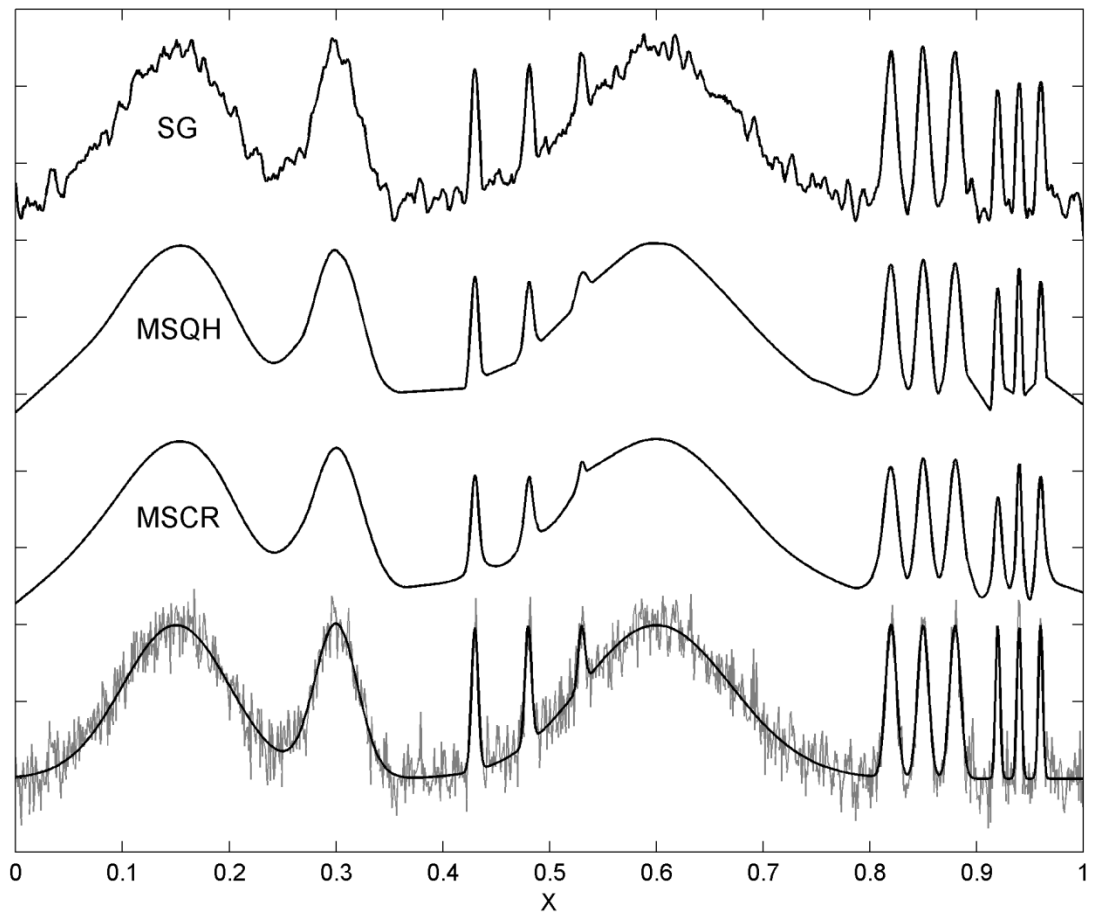


Figure 3.

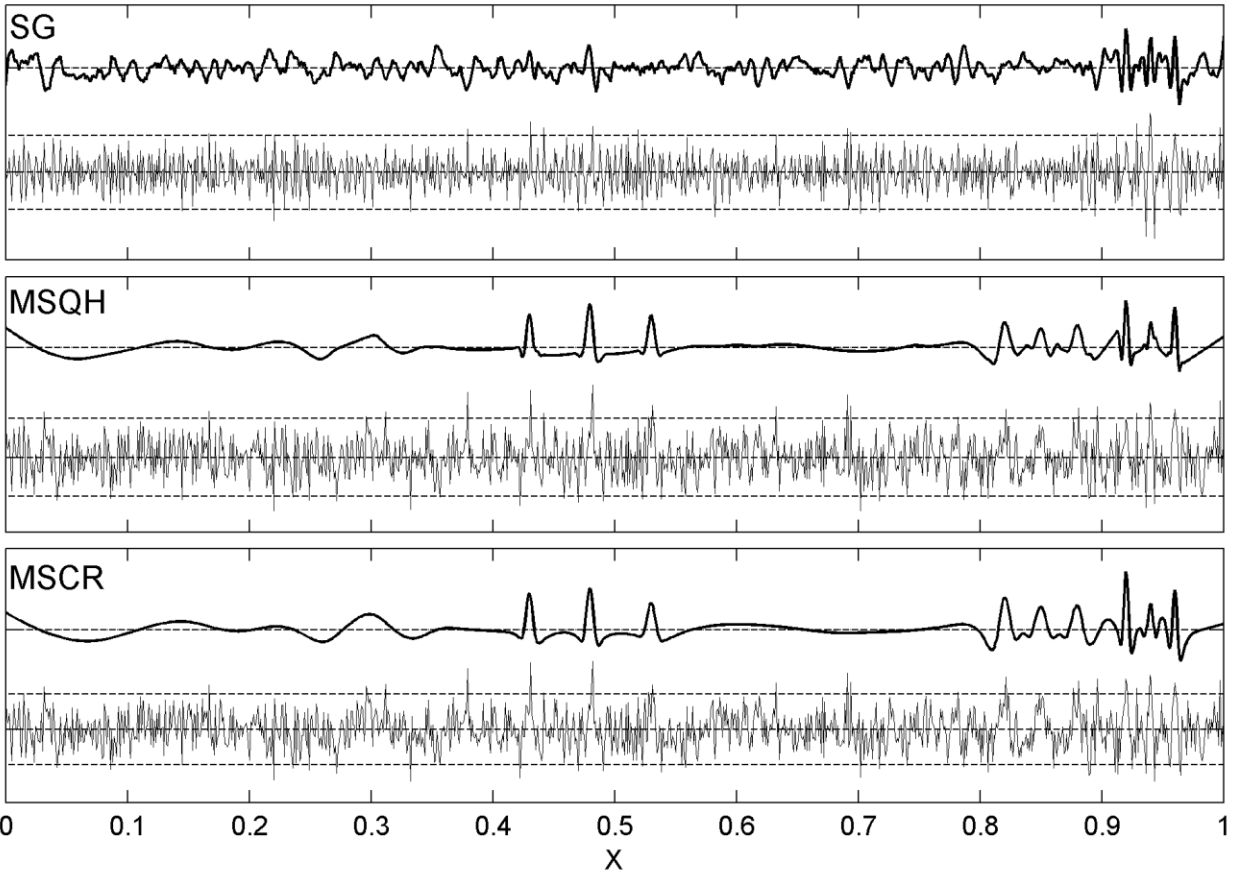


Figure 4.

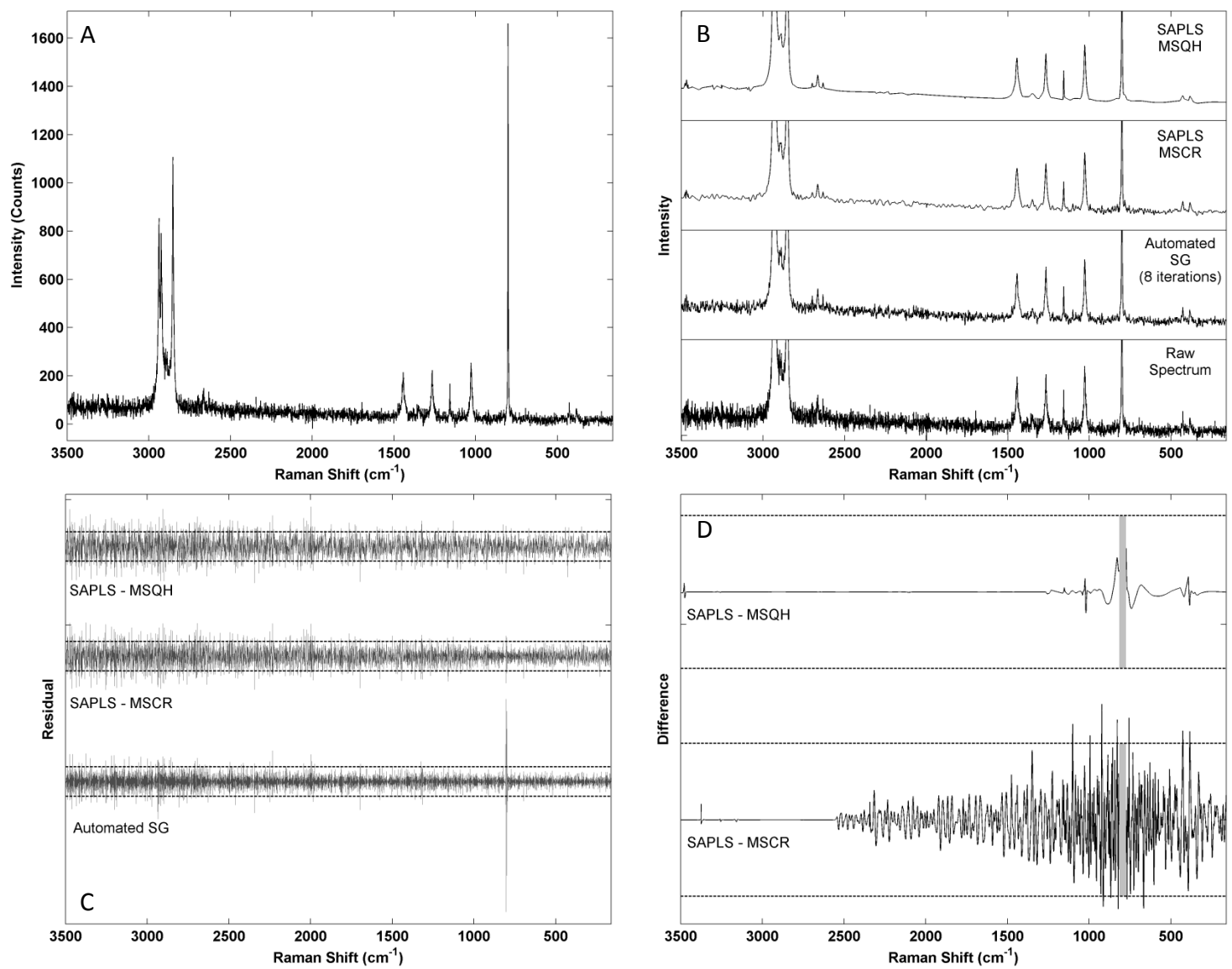


Figure 5.

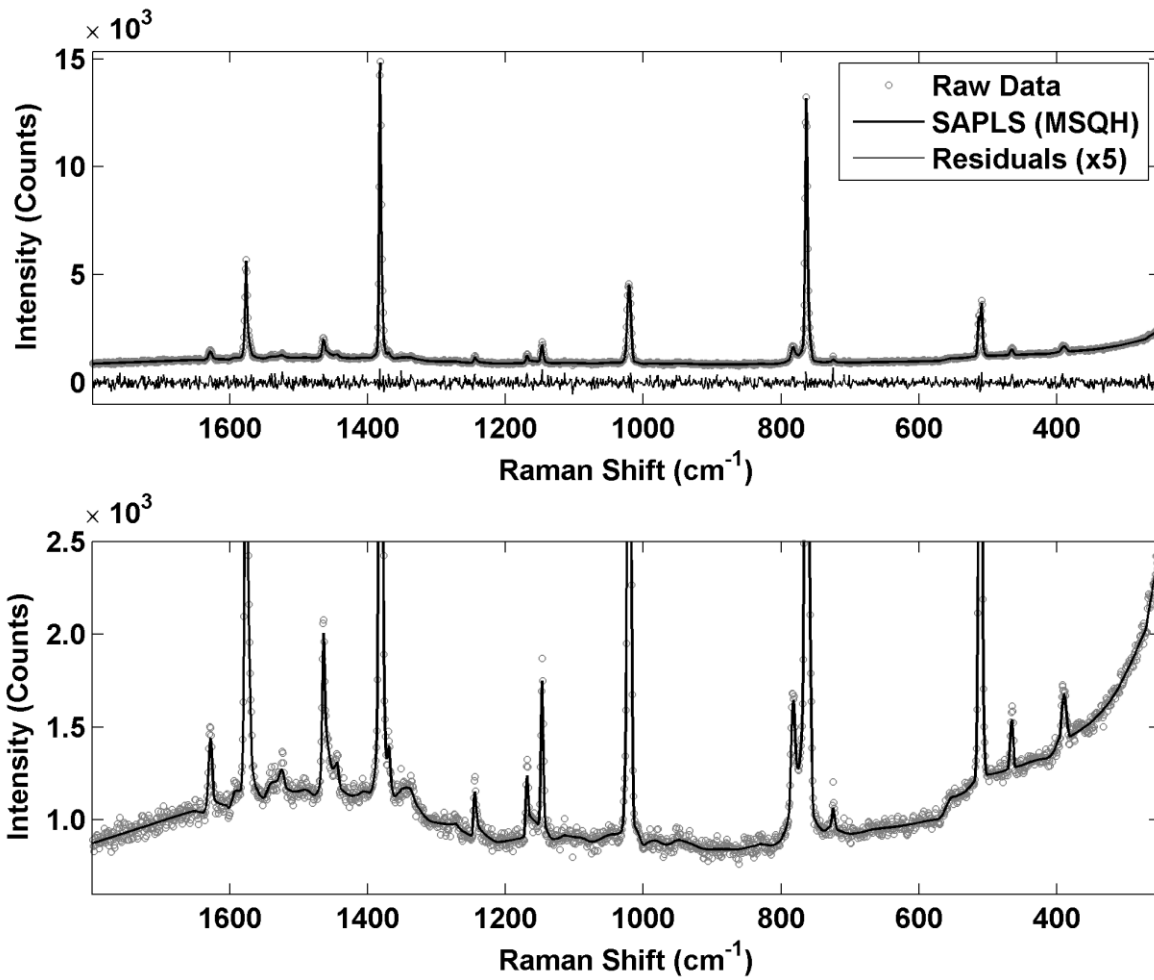


Figure 6.

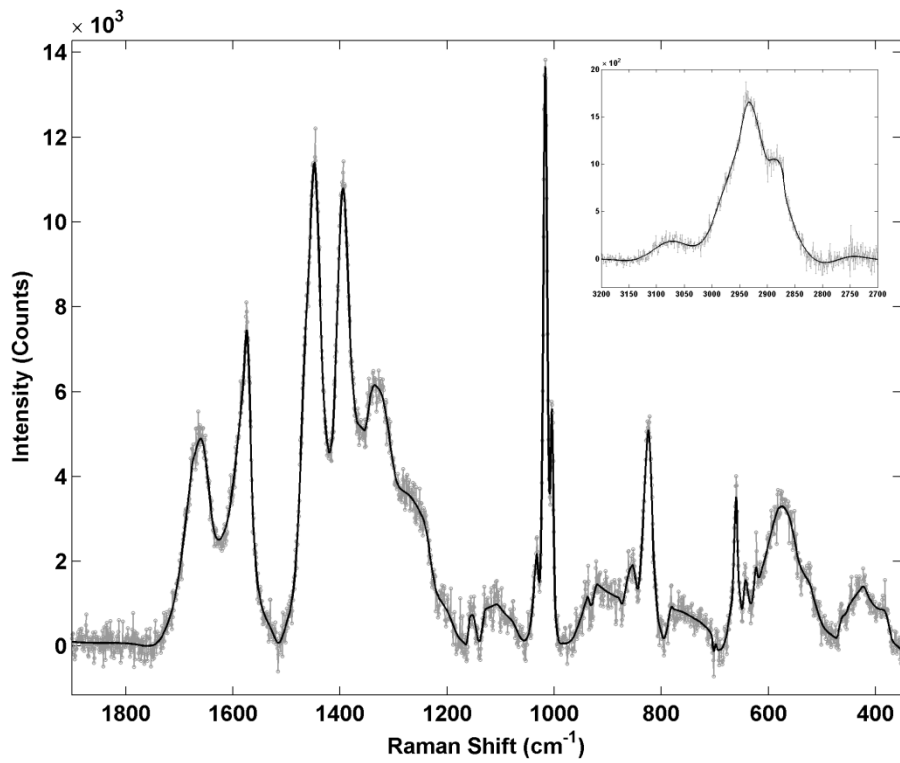
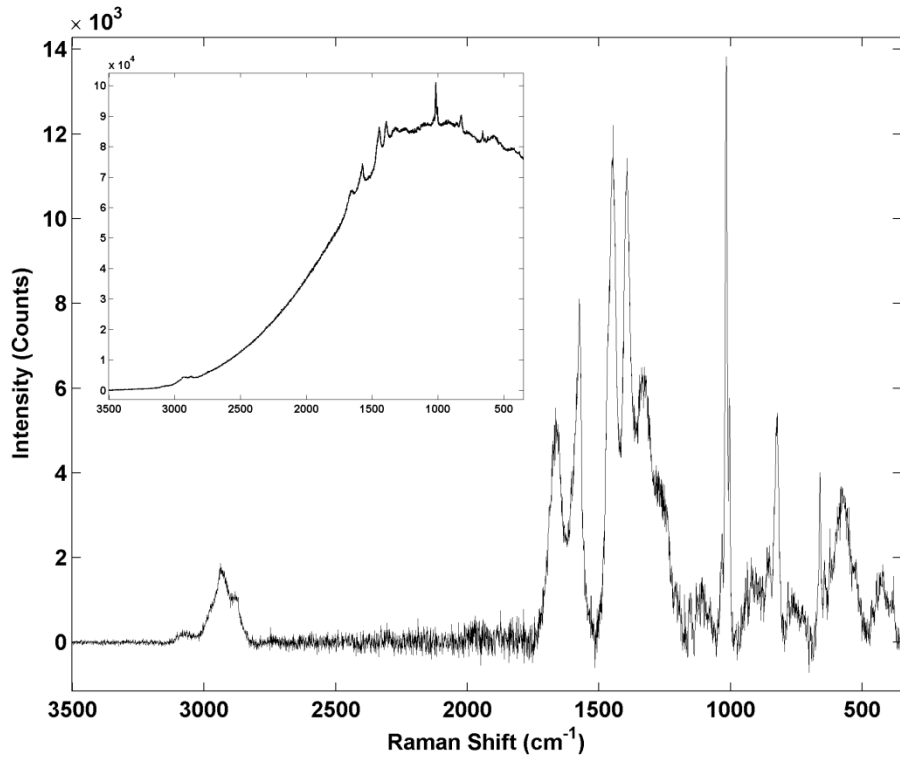


Figure 7.